Sensitivity of a prompt-gamma slit-camera to detect range shifts for proton treatment verification

Nenoff, L.; Priegnitz, M.; Janssens, G.; Petzoldt, J.; Trezza, A.; Smeets, J.; Pausch, G.; Richter, C.;

Originally published:

November 2017

Radiotherapy and Oncology 125(2017)3, 534-540

DOI: https://doi.org/10.1016/j.radonc.2017.10.013

Perma-Link to Publication Repository of HZDR:

https://www.hzdr.de/publications/Publ-25605

Sensitivity of a prompt-gamma based range verification device to different types of range shifts

Lena Nenoff[1], Marlen Priegnitz[2], Guillaume Janssens[3], Johannes Petzoldt[3], Anna Trezza[1], Julien Smeets[3], Guntram Pausch[1,4] and Christian Richter[1,4-6]

1 OncoRay – National Center for Radiation Research in Oncology, Faculty of Medicine and University Hospital Carl Gustav Carus, Technische Universität Dresden, Helmholtz-Zentrum Dresden - Rossendorf, Dresden, Germany
2 Helmholtz-Zentrum Dresden - Rossendorf, Institute for Radiation Physics, Dresden, Germany
3 Ion Beam Applications SA, Louvain-la-Neuve, Belgium
4 Helmholtz-Zentrum Dresden - Rossendorf, Institute of Radiooncology – OncoRay, Dresden, Germany
5 Department of Radiotherapy and Radiation Oncology, Faculty of Medicine and University Hospital Carl Gustav Carus, Technische Universität Dresden, Dresden, Germany
6 German Cancer Consortium (DKTK), partner site Dresden, and German Cancer Research Center (DKFZ), Heidelberg, Germany

Corresponding author:
Dr. Christian Richter, OncoRay – National Center for Radiation Research in Oncology, Faculty of Medicine and University Hospital Carl Gustav Carus, Technische Universität Dresden, PF 41, 01307 Dresden, Germany, Tel: 0049 351 458 6536, christian.richter@oncoray.de

Running head: “Sensitivity of PGI-based range verification”

Keywords: range verification, prompt gamma imaging, slit camera, proton therapy, PGI

Pages: 21
Tables: 2
Figures: 4

Abstract

Background and Purpose: Prompt-gamma imaging (PGI) was recently applied successfully in first clinical patient treatments in pencil beam scanning (PBS) and double scattering (DS). Still, systematic evaluations on its capability in clinical conditions are desirable. Here, the performance of the slit-camera is systematically assessed in well-defined error scenarios using realistic treatment deliveries to an anthropomorphic phantom.

Materials and Methods: The sensitivity to detect global and local range shifts with the slit-camera was investigated in PBS and DS irradiations of a head phantom. For PBS, measured PGI information for shifted geometries was compared spot-wise with either simulated or measured un-shifted PGI-information to evaluate the sensitivity to detect deviations from the treatment plan and interfractional shifts, respectively.

Results: Deviations from the treatment plan can be detected with an accuracy of 1.5 and 3 mm for global and local shifts in PBS, respectively. Interfractional comparisons are more affected by noise in the measurements. Evaluation of the average PGI signal of the whole field allows the detection of global shifts also in DS mode.

Conclusions: PGI-based detection of global and local range shifts under clinical conditions is possible. Especially for PBS treatments, both high sensitivity and high accuracy in shift detection were found.

Introduction

The high sensitivity of proton range to uncertainties and changes of the material in the beam path limits the precision of proton therapy [1–4]. The reduction of these uncertainties would translate into margin reductions and further reduce dose delivered to healthy tissue, which would likely increase the clinical benefit of particle therapy. Verification of the proton range in patients has been pursued as an important means to reduce range uncertainties. Along the trajectory of high-energy protons, secondary radiation is produced which can be used for non-invasive in-vivo range verification without additional dose exposition [2,3]. In contrast to secondary positron radiation [5–8], prompt-gamma radiation provides real-time information [9]. Different detection approaches resolve either energetic, temporal or spatial distribution of prompt-gamma emission, namely prompt-gamma spectroscopy[10], prompt-gamma timing [11–13] and prompt-gamma imaging (PGI) [14–18], respectively.

So far, only one prompt-gamma-based system has been applied clinically [19], the so-called PGI slit-camera [17,20]. In two patients, several fractions were monitored in DS mode without detecting any relevant range shifts. In one patient, this was in agreement with data from control CTs acquired in treatment position directly before treatment [17]. For the other patient, the control CT evaluation showed mild under- and overranges in different parts of the treatment field but no relevant shift in the PGI signal, probably due to compensation of this effect in the PGI sum-signal. The lack of spatially resolved PGI information clearly shows the general limitation of prompt-gamma based range verification in DS mode. Very recently, the first slit-camera application during a patient treatment in PBS was reported [21].

Even though the slit-camera has been intensively characterized [17,19,20,22–24], there is so far no comprehensive investigation of the general detectability of range shifts in realistic

clinical scenarios. Here, range shifts of different type and magnitude are introduced during realistic phantom irradiations and a comprehensive evaluation of the shift-detectability in different clinically relevant settings is performed.

Material and Methods

Study design

Treatment plans in DS and PBS mode for the same target volume were used. During irradiation, well-defined, laterally-limited, local range shifts, which are smaller than the lateral extension of the irradiation field and homogeneous global shifts affecting the entire lateral field were introduced and PGI profiles were measured. They were compared to either measured or simulated reference profiles without introduced shifts to investigate deviations from the nominal treatment plan or interfractional shifts, respectively.

The study design allows the evaluation of three scenarios: (a) Spotwise analysis of absolute deviations from the treatment plan in PBS (comparing a PGI measurement with a PGI simulation based on the treatment plan); (b) Spotwise analysis of interfractional shifts in PBS (comparing two measurements with and without shift); and (c) Analysis of PGI information averaged over the whole treatment field, so-called PGI sum-signal, for DS and PBS.

PGI slit-camera

The slit-camera performs a projection of the prompt-gamma distribution through a knife-edge slit-collimator on a segmented detector, allowing the measurement of a one-dimensional spatially resolved prompt-gamma distribution. It was developed by IBA (Belgium). The field of view (FOV) is approximately 10 cm along the beam axis and focused on the distal part of the target volume [17,20,23]. Even though the slit-camera was originally developed for PBS only, it can also be applied in DS [19,22]. Technical details of the

slit-camera are given in [17,20]. Range monitoring parameters were chosen as in clinical application [19,22]. The slit-camera is positioned next to the phantom, with the slit opening perpendicular to the beam. The experimental setup is presented in Figure 1.

Treatment planning and irradiation

A clinical target volume (CTV) representing a lifelike brain tumor was defined in an anthropomorphic head phantom (CIRS, USA) [25] by an experienced oncologist. The phantom consists of tissue-equivalent material with known stopping-power-ratio (SPR) used for phantom-specific CT-number-to-SPR calibration (Wohlfahrt et al, IJROBP, submitted [26]). A pseudo-monoenergetic CT (E = 79 keV) acquired with an in-room CT on rails (SOMATOM Definition AS, Siemens Healthineers, Germany) in dual-energy mode was used for treatment planning [26].

DS treatment was planned with XiO 5 (Elekta AB, Sweden). According to clinical DS protocol, dose was prescribed to the CTV, the beam was extended with a lateral margin of 3 mm and a range uncertainty margin of 3.5%+2 mm. In PBS, setup uncertainty was taken into account by extending the CTV with an isotropic setup margin of 3 mm, while range uncertainty of ±3.5% was considered in robust optimization with respect to CTV. Single-field uniform dose (SFUD) and intensity-modulated proton therapy (IMPT) treatment were calculated in RayStation 4.7 (RaySearch Laboratories AB, Sweden).

A total photon-equivalent dose of 60 Gy (considering a constant relative biological effectiveness of 1.1) with 2 Gy/fraction was prescribed to the target volume.

Only one of the two equally-weighted fields (gantry angle: 270°) was monitored. To distinguish the influence of statistical noise, an additional high-dose plan (5 Gy instead of 1 Gy/field) was calculated for each modality. All treatment plans fulfilled all clinical constraints concerning target volume coverage, chiasma and brain stem.

The experiments were performed at the clinical proton facility at OncoRay (Dresden, Germany) applying clinical dose-rate. Range shifts of known magnitude were introduced. Water-equivalent material (RW3, PTW, Germany) covering the complete beam exit was used for global shifts, for local shifts round slabs (Ø = 5 cm) of tissue-surrogate material (Gammex-RMI GmbH, Germany) were positioned at the center of the snout. Details are given in Table 1.

Data evaluation

Range differences between a measured PGI profile and a (measured or simulated) reference profile were determined using a one-dimensional least-square-matching method including Gaussian convolution as published before [27,28].

For spotwise PBS evaluation, measured PGI profiles are correlated to the corresponding spots using the treatment plan and the log-file of the treatment delivery [28]. For noise reduction, neighboring spots were aggregated with two-dimensional Gaussian smoothing (σ = 7.8 mm). Layer-average shifts for either all spots of an energy layer or only those spots, that are affected by the local shift, were calculated using spot-dose-weighting.

For the determination of range shifts between planned (simulated) and applied (measured) prompt-gamma distribution, reference profiles were simulated from the treatment plan for each PBS spot. Simulations were done with a Monte-Carlo-based analytical model [28,29]. Since the simulation neglects neutrons, a normalization of the simulated PGI counts is necessary.

Evaluation of interfractional shifts was achieved through spot-wise comparison of measurements with shifted geometry to a reference measurement without introduced shift. No normalization was applied.

Differences of layer-averaged range shifts between PGI profiles with different introduced shifts were compared by one-way ANOVA tests. Post-hoc analyses were corrected for multiple testing with the Bonferoni approach. For local shifts, differences in averaging over the complete energy layer or the shift-affected area only were tested with a two-sided paired t-test. Additionally, a one-sided t-test was performed to investigate if the detected shift differs from 0. Statistical tests were performed with SPSS 23 (IBM, USA), p-values < 0.05 were considered statistically significant.

In DS the complete laterally extended field is irradiated at once. Hence, no distinction of prompt-gamma rays from different lateral positions is possible and lateral shifts cannot be resolved per definition. For our evaluation of DS treatments, the measured time-resolved PGI signal was summed up over time, resulting in a so-called PGI sum-profile [19,22]. To generate a comparable PGI signal in PBS, sum-profiles were analogous calculated for PBS. In contrast to PBS, no dedicated tool was developed to simulate PGI data based on the treatment plan, so absolute deviations from the treatment plan cannot be assessed in DS.

Results

Spot-wise analysis in PBS

For the spatially resolved analysis of range shifts, we focus on the evaluation of IMPT 1 Gy measurements. Generally, IMPT 5 Gy and SFUD plans show similar results and are presented in Supplement A.

Maps of the determined spotwise absolute range shifts (measurement vs. simulation) are presented in Figure 2 for 6 consecutive energy layers in the FOV and all investigated shift scenarios. Shifts derived from single spots can in some cases possess large deviations from the true introduced shift due to limited count statistics. Hence, averaging neighboring spots

is advisable. The median agreement between measurement and simulation (both without shifts) was found to be better than 1 mm for layer-averaged evaluation, underlining the accuracy of the implemented analytical PGI simulation (Figure 3a). Also, one-sided t-tests proved no significant range difference. Introduced global shifts are clearly visible in all layers, the detected layer-averaged shifts differ significantly from 0 and are in agreement with the expectation (introduced shift length in brain material) with an accuracy of 1.5 mm. The differences of detected shifts between different introduced global shifts are statistically significant. For local shifts, spots with the center of gravity within a radius of 2.5 cm from the central beam axis are considered to be affected by the shift. The corresponding area can be distinguished from the surrounding area with statistical significance. Nevertheless, range mixing occurs at the edge of local shifts for spots that only partly cover the shifted area. Therefore, average differences of local shifts (clustered in the shifted region only) are slightly underestimated. Still, the shift detection accuracy is 3 mm.

Shift-maps for the interfractional analysis comparing two measurements with and without introduced shifts are presented in Supplement B. In contrast to the comparison of measurement with simulation, here the reference measurement (without shift) is also affected by statistical noise, resulting in higher standard deviations of the detected shifts (Figure 3b). Introduced global shifts are quantitatively detectable, with layer-averaged PGI information an accuracy of 3 mm was reached. All detected layer-averaged shifts, except the local 10 mm shift, differed significantly from 0. The low precision (increased standard deviations) of interfractional local shifts limits their general detectability. Visually, local shifts can only be identified in high-weighted energy layers.

Comparison of DS and PBS: Analysis of sum-profiles

The evaluation of the sum-profiles for different treatment modalities is presented in Figure 4. Global shifts can be detected with an accuracy of 1 mm for all treatment modalities. Even though the sum-profiles allow no laterally-resolved analysis of local range shifts, the detected shift is increasing with increasing introduced shifts (Figure 4c).

Overview of all results

In Table 2, a summary of the shift-detection sensitivity for the presented PGI signal evaluation is given for all investigated scenarios. Generally, a comparison of measured PGI profiles with shifted geometry with a reference simulation (absolute shift) is more accurate than a comparison with a reference measurement (interfractional shift). The comparison with simulations is more relevant for clinical application as it relates the shift to the treatment plan. No relevant difference in shift detection sensitivity was found between the IMPT and SFUD. Range shift detection for clinical relevant doses (1 Gy/field) is feasible. An increase of the dose from 1 to 5 Gy slightly improves the accuracy of interfractional global shift determination, whereas the accuracy of the comparison of measurement and simulation is not improved. In fact, with this dose escalation the detection accuracy of interfractional layer-averaged global shifts is comparable with the comparison to simulations.

Discussion

The sensitivity to detect range shifts with the slit-camera in a realistic clinical scenario was investigated for different types of range shifts, beam delivery techniques and evaluation methods. In general, not only a high sensitivity, but also a high accuracy of shift detection was reached in different scenarios. Therefore, a routine application for shift detection in clinical treatments, especially in PBS, is promising.

For the most clinical relevant evaluation method, the comparison of PGI measurements with treatment-plan-based simulations in PBS mode, the highest accuracy was reached. This is not only due to the fact that noise in measurements has less influence than for the interfractional scenario, also an accurate simulation of the PGI profile is crucial. Both, the reached simulation accuracy (1 mm for an isotropic grid size of 1 mm) as well as the reached shift detection accuracy for realistic treatment scenarios, prove the clinical applicability of the slit-camera. Also local shifts can be clearly distinguished from unaffected regions.

The interfractional evaluation comparing two measurements reveals information about patient setup and anatomy, but is completely independent from planning CT, CT-based stopping-power prediction, PGI simulation and any uncertainties related to them. On the other hand it is also more prone to noise in the PGI measurement leading to slightly reduced shift detection accuracy. Hence, it is recommended to limit the evaluation to high-intensity spots. In this study, the setup of phantom and slit-camera was not changed assuming perfect reproducibility in patient and camera positioning at different days. In clinical practice, interfractional evaluations can be a helpful, supplemental tool to evaluate the influence of potential anatomical changes during treatment and to exclude influences from non-perfect CT-based simulations. Careful comparison of treatment-plan-based and interfractional shift information detected on different days could help to distinguish the reasons of range difference.

Generally, the low number of protons per spot limits the precision of shift detection. Clustering neighbored spots is always a compromise between lateral resolution and accuracy. Here the position and size of the local shift is known, so respective spots can be clustered separately. In clinical application this would not be possible without information from an additional control CT. Nevertheless, it was shown that local range shifts can be

detected visually in the presented shift-maps, as well as qualitatively evaluating layer-averaged shifts. From this information a warning flag could be generated that triggers further investigation, e.g. further CT imaging and dose recalculation. In addition, more sophisticated methods of spot clustering are possible. For example, clustering could by constrained to reach the same counting statistics for each cluster to achieve the same measurement uncertainty. Alternatively, clustering based on anatomical structures or organs at risks close to the target volume is possible.

The detection of local shifts is depending on lateral size and magnitude of the shifts: The smaller the affected area and magnitude of the shift, the more difficult its detection. Here only one size of local shifts, but three different magnitudes were investigated. Further studies could extend this parameter space.

As also shown here, an evaluation of sum-profiles is possible in DS and PBS. In DS this is the method of choice, whereas in PBS more sophisticated methods, such as spot-wise shift detection, are available. Nevertheless, sum-profile evaluation is helpful to detect global or severe shifts and indicate the necessity of further imaging.

An additional limitation of this study is the quantification of expected shifts, which was estimated with the equivalent shift in the phantom´s brain material. This simplification neglects bony material in the target volume. Nevertheless it is reasonable, because the main part of the target volume, especially the most distal high-weighted energy layers are predominantly located in brain material.

As a next step, a systematic clinical application of the slit-camera in PBS mode for different entities, e.g. prostate or head and neck, is planned. Per target region, at least 10 patients should be monitored with PGI range-verification over the complete treatment course,

accompanied by in-room control CT-imaging, to derive a deeper understanding of the correlation of the detected PGI fingerprint with anatomical or setup changes. Currently an upgrade of the camera trolley is in preparation allowing a high level of day-to-day reproducibility in camera positioning (≤ 1 mm).

Conclusion

PGI-based detection of global and local range shifts (investigated shift thickness of ≥4 mm) is possible under realistic clinical conditions. Especially for PBS treatments, both high sensitivity and high accuracy in shift detection were found. More sophisticated clustering of PGI information from neighbor spots could further improve the shift detection capability.

Acknowledgements

This work was partly founded by the Federal Ministry of Education and Research – Germany (BMBF-03Z1N51, BMBF-03Z1NN12). Johannes Petzoldt is funded from a EU-Horizon2020 Marie-Sklodowska-Curie grant (#675265, "Optimization of Medical Accelerators"). The Author´s would like to thank Patrick Wohlfahrt and Steffen Löck for CT data processing and statistical analysis, respectively. François Vander Stappen and Lucian Hotoiu are acknowledged for helpful discussions and precious support.

Conflict of interest

This study is part of an institutional research agreement between OncoRay, HZDR and IBA. The research position of Lena Nenoff benefited from partial, bridge funding by IBA for completion of this study, under sole supervision of OncoRay.

References

[1] Baumann M, Krause M, Overgaard J, Debus J, Bentzen SM, Daartz J, et al. Radiation oncology in the era of precision medicine. Nat Rev Cancer 2016;16:234–49.

[2] Knopf A-C, Lomax A. In vivo proton range verification: a review. Phys Med Biol 2013;58:R131-

160.

[3] Kraan AC. Range Verification Methods in Particle Therapy: Underlying Physics and Monte Carlo Modeling. Front Oncol 2015;5:1–27.

[4] Paganetti H. Range uncertainties in proton therapy and the role of Monte Carlo simulations. Phys Med Biol 2012;57:R99-117.

[5] Enghardt W, Crespo P, Fiedler F, Hinz R, Parodi K, Pawelke J, et al. Charged hadron tumour therapy monitoring by means of PET. Nucl Instruments Methods Phys Res A 2004;525:284–8.

[6] Parodi K, Enghardt W, Haberer T. In-beam PET measurements of β+ radioactivity. Phys Med Biol 2002;47:21–36.

[7] Zhu X, España S, Daartz J, Liebsch N, Ouyang J, Paganetti H, et al. Monitoring proton radiation therapy with in-room PET imaging. Phys Med Biol 2011;56:4041–57.

[8] Attanasi F, Knopf A, Parodi K, Paganetti H, Bortfeld T, Rosso V, et al. Extension and validation of an analytical model for in vivo PET verification of proton therapy - a phantom and clinical study. Phys Med Biol 2011;56:5079–98.

[9] Min CH, Kim CH, Youn MY, Kim JW. Prompt gamma measurements for locating the dose falloff region in the proton therapy. Appl Phys Lett 2006;89:18357-1–3.

[10] Verburg JM, Seco J. Proton range verification through prompt gamma-ray spectroscopy. Phys Med Biol 2014;59:7089–106.

[11] Petzoldt J, Roemer KE, Enghardt W, Fiedler F, Golnik C, Hueso-González F, et al. Characterization of the microbunch time structure of proton pencil beams at a clinical treatment facility. Phys Med Biol 2016;61:2432–56.

[12] Golnik C, Hueso-González F, Müller A, Dendooven P, Enghardt W, Fiedler F, et al. Range assessment in particle therapy based on prompt γ-ray timing measurements. Phys Med Biol 2014;59:5399–422.

[13] Hueso-Gonzales F, Enghardt W, Fiedler F, Golnik C, Janssens3 G, Petzoldt J, et al. First test of the prompt gamma ray timing method with heterogeneous targets at a clinical proton therapy facility. Phys Med Biol 2015;60:6247 – 6272.

[14] Robertson D, Polf JC, Peterson SW, Gillin MT, Beddar S. Material efficiency studies for a Compton camera designed to measure characteristic prompt gamma rays emitted during proton beam radiotherapy. Phys Med Biol 2011;56:3047–59.

[15] Park JH, Seo H, Kim YS, Kim CH, Lee JH, Lee CS, et al. Monte Carlo simulations on performance of double-scattering Compton camera. J Instrum 2012;7:C01009–C01009.

[16] Hueso-Gonzalez F, Golnik C, Berthel M, Dreyer A, Enghardt W, Fiedler F, et al. Test of a compton imaging prototype at the ELBE bremsstrahlung beam. J Instrum 2014.

[17] Smeets J, Roellinghoff F, Prieels D, Stichelbaut F, Benilov A, Busca P, et al. Prompt Gamma Imaging with a slit camera for real-time range control in proton therapy. Phys Med Biol 2012;57:3371–405.

[18] Bom V, Joulaeizadeh L, Beekman F. Real-time prompt gamma monitoring in spot-scanning proton therapy using imaging through a knife-edge-shaped slit. Phys Med Biol 2011;57:297–308.

[19] Richter C, Pausch G, Barczyk S, Priegnitz M, Keitz I, Thiele J, et al. First clinical application of a prompt gamma based in vivo proton range verification system. Radiother Oncol 2016:1–6.

[20] Perali I, Celani A, Bombelli L, Fiorini C, Camera F, Clementel E, et al. Prompt gamma imaging of proton pencil beams at clinical dose rate. Phys Med Biol 2014;59:5849–71.

[21] Xie Y, Bentefour H, Janssens G, Smeets J, Stappen F Vander, Hotoiu L, et al. Prompt gamma imaging for in vivo range verification of pencil beam scanning proton therapy. Int J Radiat Oncol 2017.

[22] Priegnitz M, Barczyk S, Nenoff L, Golnik C, Keitz I, Werner T, et al. Towards clinical application: prompt gamma imaging of passively scattered proton fields with a knife-edge slit camera. Phys Med Biol 2016;61:7881–905.

[23] Priegnitz M, Helmbrecht S, Janssens G, Perali I, Smeets J, Vander Stappen F, et al. Detection of mixed-range proton pencil beams with a prompt gamma slit camera. Phys Med Biol 2016;60:855–71.

[24] Priegnitz M, Helmbrecht S, Janssens G, Perali I, Smeets J, Vander Stappen F, et al. Measurement of prompt gamma profiles in inhomogeneous targets with a knife-edge slit camera during proton irradiation. Phys Med Biol 2015;60:4849–71.

[25] Albertini F, Casiraghi M, Lorentini S, Rombi B, Lomax a J. Experimental verification of IMPT treatment plans in an anthropomorphic phantom in the presence of delivery uncertainties. Phys Med Biol 2011;56:4415–31.

[26] Wohlfahrt P, Möhler C, Hietschold V, Menkel S, Greilich S, Krause M, et al. Clinical implementation of dual-energy CT for proton treatment planning on pseudo-monoenergetic CT scans. Int J Radiat Oncol • Biol • Phys 2016.

[27] Helmbrecht S, Enghardt W, Fiedler F, Iltzsche M, Pausch G, Tintori C, et al. In-beam PET at clinical proton beams with pile-up rejection. Zeitschrift Für Medizinische Phys 2016:1–16.

[28] Janssens G, Smeets J, Vander F, Prieels D, Clementel E, Hotoiu E, et al. Sensitivity study of prompt gamma imaging of scanned beam proton therapy in heterogeneous anatomies. Radiother Oncol 2015:1–6.

[29] Sterpin E, Janssens G, Smeets J, Vander Stappen F, Prieels D, Priegnitz M, et al. Analytical computation of prompt gamma ray emission and detection for proton range veri fi cation. Phys Med Biol 2015;60:4915–4946.

Figure legends

Figure 1 a) Experimental setup with head phantom and slit-camera. The slit is oriented perpendicular to the beam. Range shifts were introduced at the snout exit downstream to the range shifter, centered at the central beam axis. b) Transversal CT slice of the head phantom with CTV contour and dose of the monitored beam of the IMPT plan.

Figure 2 Detected range shifts by comparing PGI measurement and simulation for separate spots in 6 consecutive energy layers. Spot size correlates with the number of protons. For each layer, the layer-averaged shift and its standard deviation are given. The black circle marks the area where the local shift was introduced. For local shifts, mean and its standard deviation are given separately in- and outside the affected area.

Figure 3 Distribution of the layer-averaged shifts (whole layer or region inside the shift-affected area) over all investigated energy layers. Significant differences ($p<0.05$, black: ANOVA; grey: paired t-test) are marked with *.

Figure 4 Range shifts detected from PGI sum-profiles.

Table 1 Introduced global and local shifts in water and brain tissue surrogate.

Acronym	Type	Shift in water/mm	Shift in brain/mm
G-10	global	10.3	9.9
G-7	global	7.2	6.9
G-5	global	5.2	5.0
L-10	local	10.4	10.0
L-7	local	7.4	7.1
L-4	local	4.0	4.0

Table 2 Overall assessment of the shift-detection accuracy, Median (σ_{mean}) in mm. For fast overview, three groups were defined: Green: median+σ ≤ 2 mm, blue: > 2 mm, ≤ 4 mm, yellow: > 4 mm. The assessment is based on layer-averaged shifts. Grey numbers with a * show differences ≤ 1 mm based on the sum-profile. Cases marked with "-" were not investigated.

Technique	Dose/Gy	Absolute (measurement vs simulation)		Interfractional (measurement vs measurement)	
		Global	Local	Global	Local
IMPT	1	**0.9 (σ < 0.7)**	**2.3 (σ < 0.8)**	**1.8 (σ < 0.6)**	**3.4 (σ < 2.1)**
	5	**0.6 (σ < 0.8)**	**1.9 (σ < 0.8)**	**0.8 (σ < 0.5)**	**2.0 (σ < 0.9)**
SFUD	1	**1.4 (σ < 0.8)**	**1.7 (σ < 0.9)**	**2.0 (σ < 1.1)**	**1.9 (σ < 3.1)**
	5	**1.5 (σ < 0.5)**	**1.6 (σ < 0.7)**	**0.9 (σ < 0.8)**	**0.9 (σ < 3.4)**
DS	1	-	-	**0.7***	-
	5	-	-	**0.6***	-

Figure 1:

380

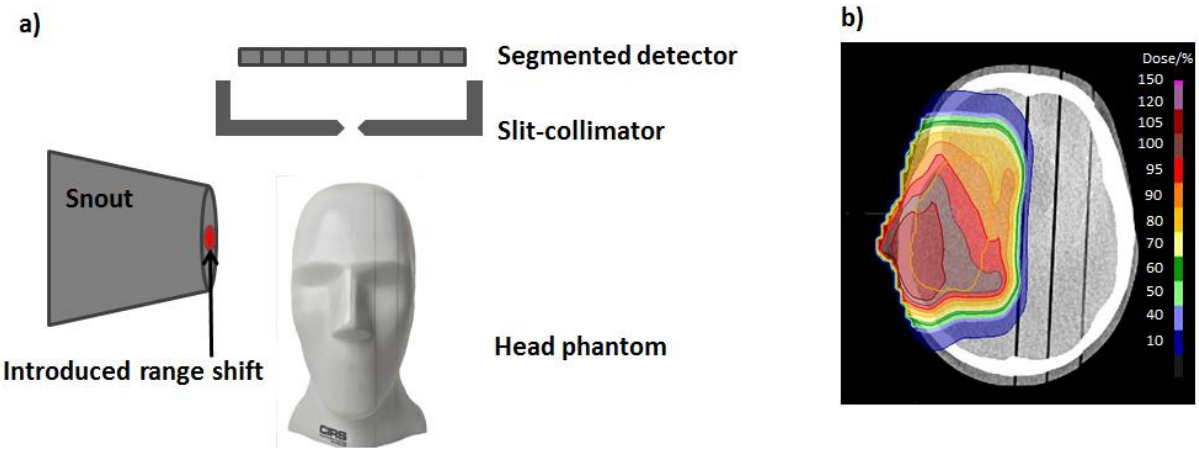
a)
Segmented detector
Slit-collimator
Snout
Introduced range shift
Head phantom
b)
Dose/%
150
120
105
100
95
90
80
70
60
50
40
10

Figure 2

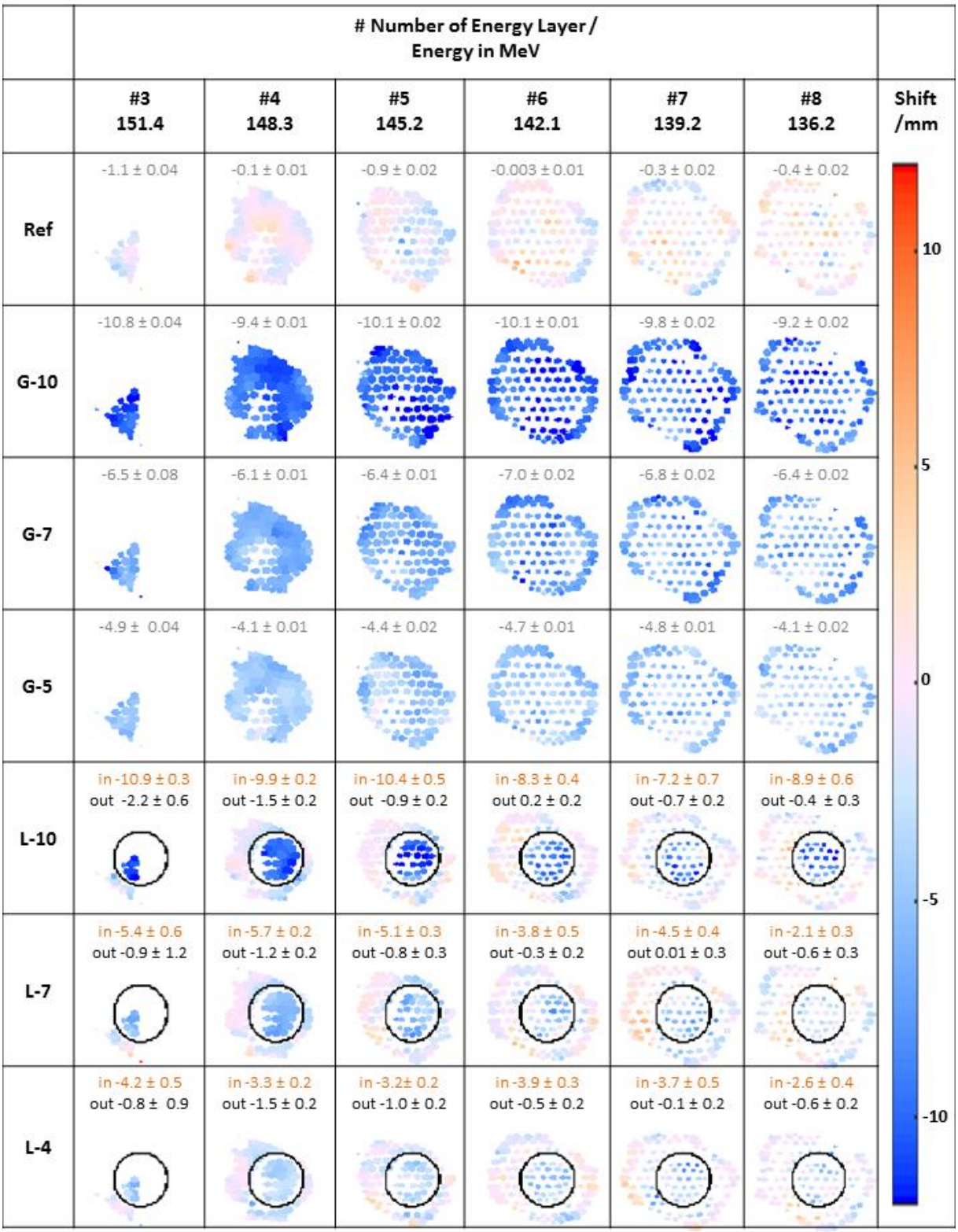
Number of Energy Layer / Energy in MeV
#3 151.4
#4 148.3
#5 145.2
#6 142.1
#7 139.2
#8 136.2
Shift /mm
10
5
0
-5
-10
Ref
-1.1 ± 0.04
-0.1 ± 0.01
-0.9 ± 0.02
-0.003 ± 0.01
-0.3 ± 0.02
-0.4 ± 0.02
G-10
-10.8 ± 0.04
-9.4 ± 0.01
-10.1 ± 0.02
-10.1 ± 0.01
-9.8 ± 0.02
-9.2 ± 0.02
G-7
-6.5 ± 0.08
-6.1 ± 0.01
-6.4 ± 0.01
-7.0 ± 0.02
-6.8 ± 0.02
-6.4 ± 0.02
G-5
-4.9 ± 0.04
-4.1 ± 0.01
-4.4 ± 0.02
-4.7 ± 0.01
-4.8 ± 0.01
-4.1 ± 0.02
L-10
in -10.9 ± 0.3 out -2.2 ± 0.6
in -9.9 ± 0.2 out -1.5 ± 0.2
in -10.4 ± 0.5 out -0.9 ± 0.2
in -8.3 ± 0.4 out 0.2 ± 0.2
in -7.2 ± 0.7 out -0.7 ± 0.2
in -8.9 ± 0.6 out -0.4 ± 0.3
L-7
in -5.4 ± 0.6 out -0.9 ± 1.2
in -5.7 ± 0.2 out -1.2 ± 0.2
in -5.1 ± 0.3 out -0.8 ± 0.3
in -3.8 ± 0.5 out -0.3 ± 0.2
in -4.5 ± 0.4 out 0.01 ± 0.3
in -2.1 ± 0.3 out -0.6 ± 0.3
L-4
in -4.2 ± 0.5 out -0.8 ± 0.9
in -3.3 ± 0.2 out -1.5 ± 0.2
in -3.2± 0.2 out -1.0 ± 0.2
in -3.9 ± 0.3 out -0.5 ± 0.2
in -3.7 ± 0.5 out -0.1 ± 0.2
in -2.6 ± 0.4 out -0.6 ± 0.2

385

Figure 3

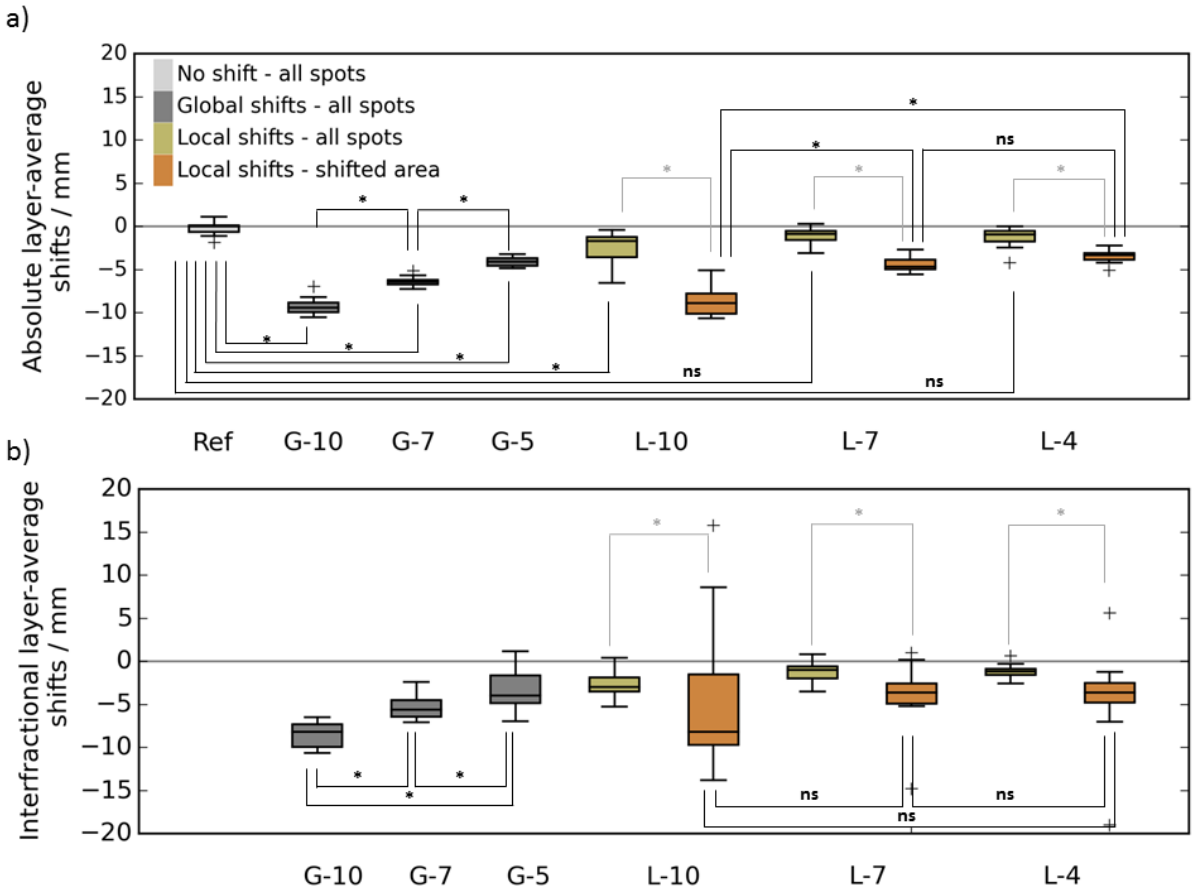
a)
No shift - all spots
Global shifts - all spots
Local shifts - all spots
Local shifts - shifted area
Absolute layer-average shifts / mm
20
15
10
5
0
−5
−10
−15
−20
*
ns
Ref
G-10
G-7
G-5
L-10
L-7
L-4
b)
Interfractional layer-average shifts / mm
20
15
10
5
0
−5
−10
−15
−20
*
ns
G-10
G-7
G-5
L-10
L-7
L-4

390 Figure 4:

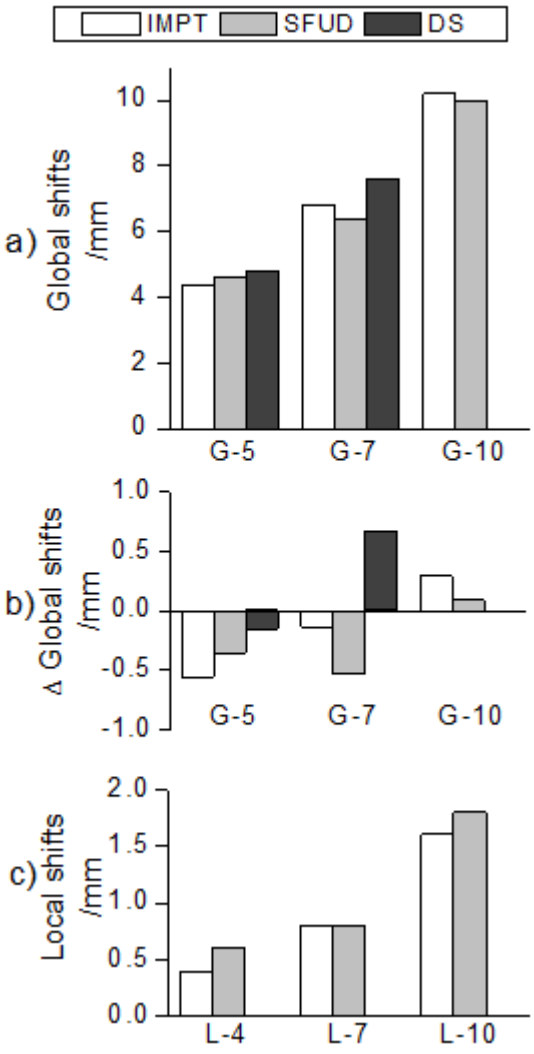
IMPT
SFUD
DS
a)
Global shifts /mm
10
8
6
4
2
0
G-5
G-7
G-10
b)
Δ Global shifts /mm
1.0
0.5
0.0
-0.5
-1.0
G-5
G-7
G-10
c)
Local shifts /mm
2.0
1.5
1.0
0.5
0.0
L-4
L-7
L-10

Table 1

Table 1 Introduced global and local shifts in water and brain tissue surrogate.

Acronym	Type	Shift in water/mm	Shift in brain/mm
G-10	global	10.3	9.9
G-7	global	7.2	6.9
G-5	global	5.2	5.0
L-10	local	10.4	10.0
L-7	local	7.4	7.1
L-4	local	4.0	4.0

Table 2

Table 1 Overall assessment of the shift-detection accuracy, Median (σ_{mean}) in mm. For fast overview, three groups were defined: Green: median+σ ≤ 2 mm, blue: > 2 mm, ≤ 4 mm, yellow: > 4 mm. The assessment is based on layer-averaged shifts. Grey numbers with a * show differences ≤ 1 mm based on the sum-profile. Cases marked with "-" were not investigated.

Technique	Dose/Gy	Absolute (measurement vs simulation)		Interfractional (measurement vs measurement)	
		Global	Local	Global	Local
IMPT	1	**0.9 (σ < 0.7)**	**2.3 (σ < 0.8)**	**1.8 (σ < 0.6)**	**3.4 (σ < 2.1)**
	5	**0.6 (σ < 0.8)**	**1.9 (σ < 0.8)**	**0.8 (σ < 0.5)**	**2.0 (σ < 0.9)**
SFUD	1	**1.4 (σ < 0.8)**	**1.7 (σ < 0.9)**	**2.0 (σ < 1.1)**	**1.9 (σ < 3.1)**
	5	**1.5 (σ < 0.5)**	**1.6 (σ < 0.7)**	**0.9 (σ < 0.8)**	**0.9 (σ < 3.4)**
DS	1	-	-	**0.7***	-
	5	-	-	**0.6***	-

Figure 1
Click here to download high resolution image

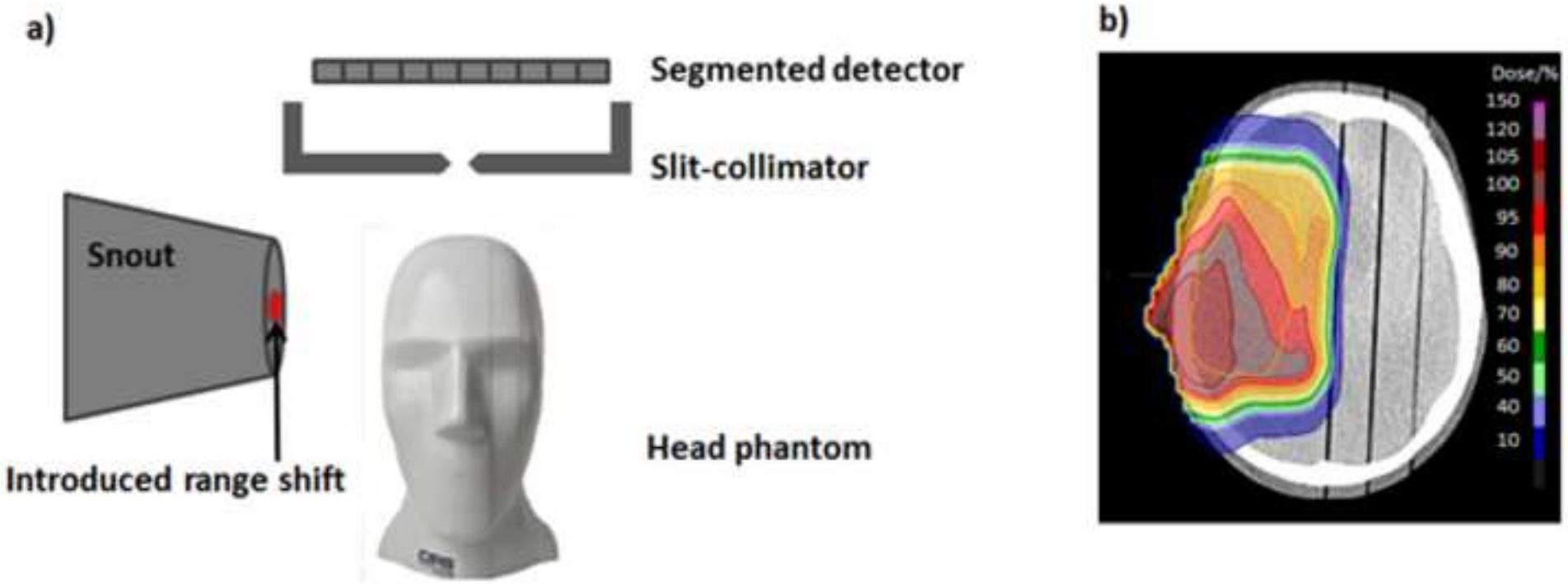

Figure 2

Click here to download high resolution image

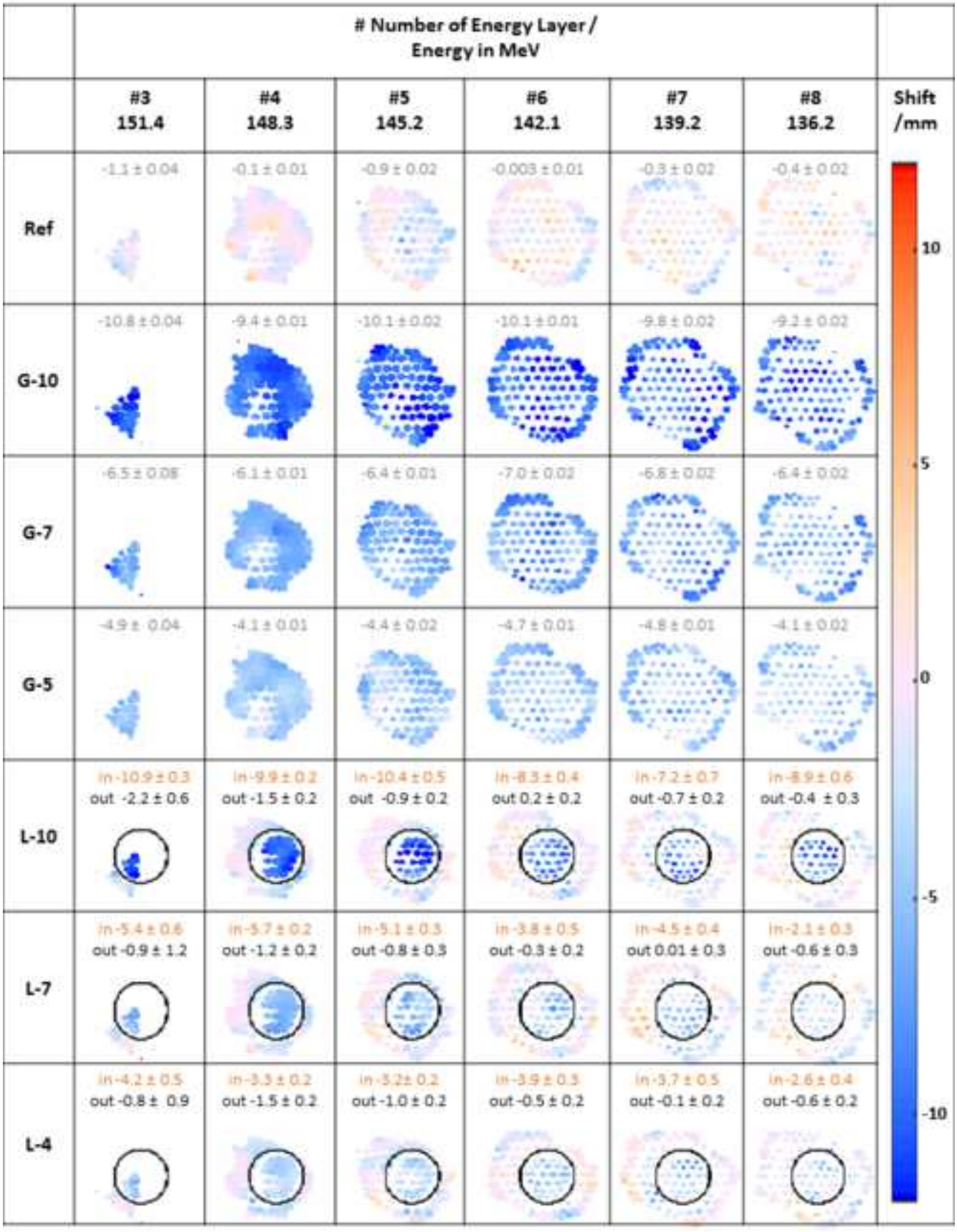

Figure 3

Click here to download high resolution image

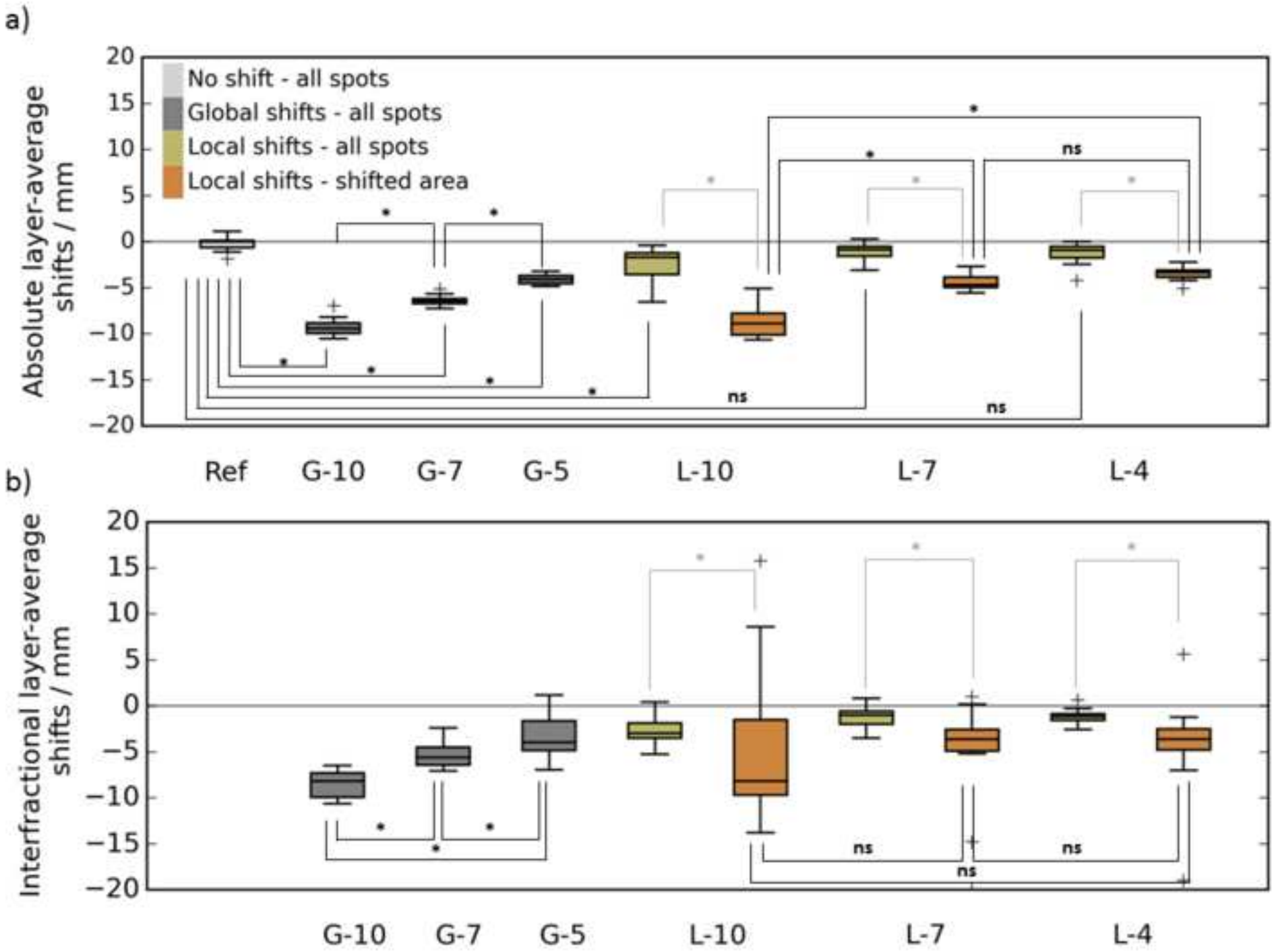

Figure 4

Click here to download high resolution image

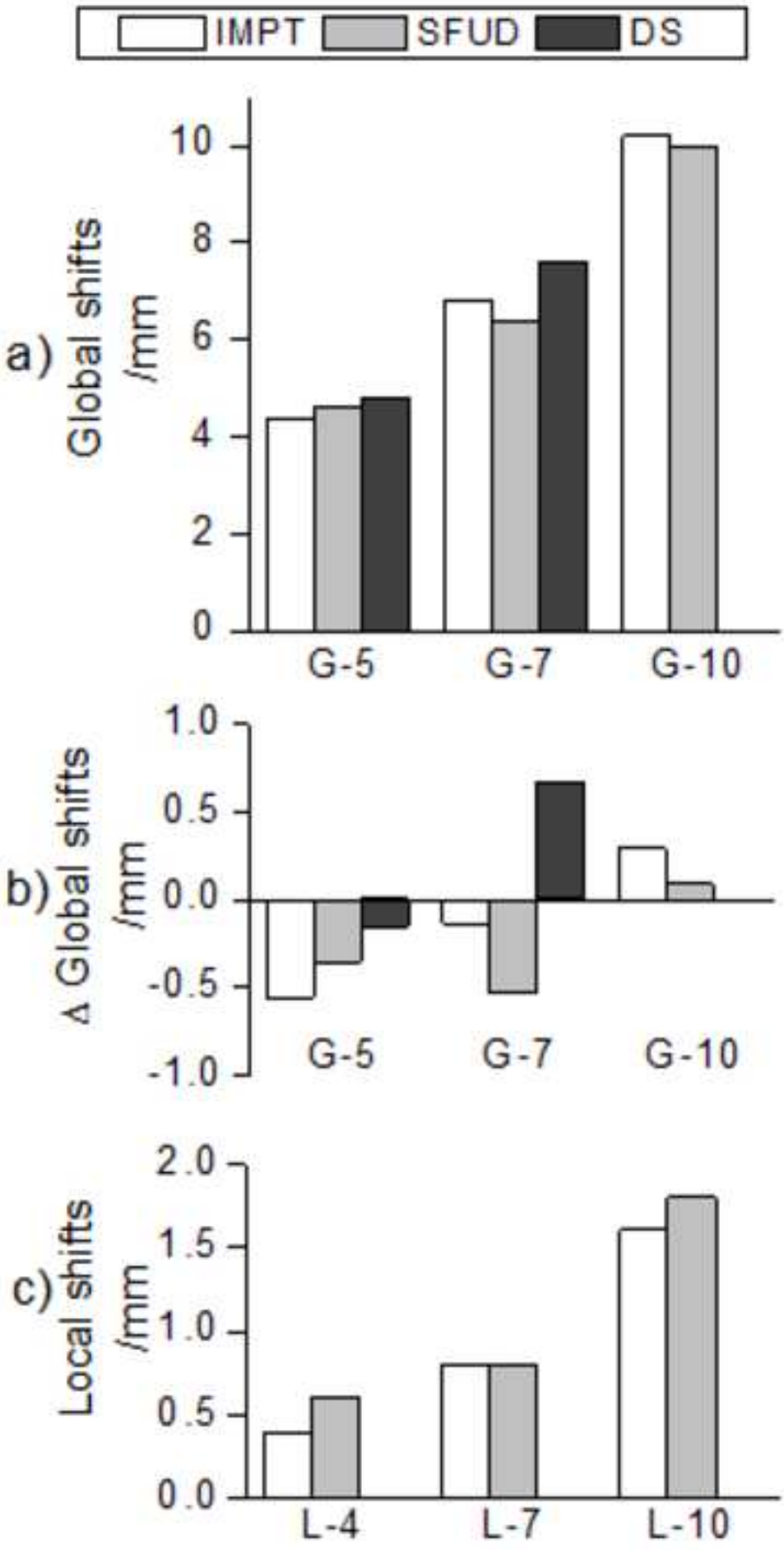

Supplementary Files

Click here to download Supplementary Files: supplement_final_2017-05-30_submitted.docx

Conflict of interest

This study is part of an institutional research agreement between OncoRay, HZDR and IBA. The research position of Lena Nenoff benefited from partial, bridge funding by IBA for completion of this study, under sole supervision of OncoRay.